J Mater Sci (2010) 45:911–918
DOI 10.1007/s10853-009-4020-8

Role of strain-induced martensite on microstructural evolution during annealing of metastable austenitic stainless steel

B. Ravi Kumar · S. K. Das · B. Mahato · R. N. Ghosh

Received: 16 February 2009 / Accepted: 5 November 2009 / Published online: 21 November 2009

Abstract Metastable austenitic stainless steel of type AISI 304L was cold rolled to 90% with and without inter-pass cooling. Inter-pass cooling produced 89% of strain-induced martensite whereas no inter-pass cooling resulted in the formation of 43% of martensite in the austenite matrix. The cold-rolled specimens were annealed at various temperatures in the range of 750–1000 °C. The microstructures of the cold-rolled and annealed specimens were studied by the electron microscope. The grain size and low angle boundaries were determined from the orientation maps recorded by the scanning electron microscope-based electron backscattered diffraction technique. The observed microstructural changes were correlated with the reversion mechanism of martensite to austenite and volume fraction of martensite. It was noted that large volume fractions of martensite at low annealing temperatures, below 900 °C, were most suitable for the formation of fine grains. On the contrary, reversion of small volume fractions of martensite at critical annealing temperature of 950 °C resulted in grain refinement.

Introduction

Grain refinement is an important mechanism to improve the both strength and toughness of structural steels. In the recent past, new approaches were adopted to enhance the properties by reducing the grain size to nano structures/grain ($d < 100$ nm) and ultrafine-grain ($d < 500$ nm) in polycrystalline materials. These materials were expected to possess superior mechanical properties as compared to their coarse-grained counterparts. The commonly used laboratory techniques for producing ultrafine-grain (ufg) steels utilise two approaches: Severe Plastic Deformation (SPD) techniques and advanced thermomechanical processing. For the production of ufg steel with an average grain size below 1 μm through SPD techniques, large accumulated plastic strains are required [1–14]. Typical SPD techniques include Equal-channel Angular Pressing (ECAP) [4–10], Accumulative Roll-bonding (ARB) [11–13] and bi-directional compression [14]. The small scale complexity and the batch nature of SPD methods suggest application to high volume steel production may not be feasible. In contrast to SPD, advanced thermomechanical processes exploit the dynamic recrystallization of austenite during hot deformation with the subsequent austenite to ferrite transformation [15], strain-induced ferrite transformation [16–19], hot rolling in the inter critical region [20] or cold rolling and annealing of martensite phase [21–25]. Advanced thermomechanical methods are large-scale industrial processes and can be more readily optimised as compared to SPD techniques. A recent novel route of forming ufg/nano grain (ng) metastable austenitic stainless steels (SS) involves annealing of heavily cold-worked SS [26–29]. In this process, during the cold rolling, metastable austenite was transformed to strain-induced martensite. The grain refining annealing process results in near complete transformation of strain-induced martensite to austenite. The reversion of strain-induced martensite to austenite takes place over a temperature range of 450–800 °C, exhibiting marked austenite grain refinement [26–37]. The early researchers mainly focused on the kinetics of the strain-induced phase transformation during deformation. The more recent work focused on the microstructural aspects of the reverted austenite. The microstructural

B. Ravi Kumar (✉) · S. K. Das · B. Mahato · R. N. Ghosh
Materials Science and Technology Division, National Metallurgical Laboratory, CSIR, Jamshedpur, India
e-mail: ravik@nmlindia.org

changes were mostly correlated to the two reversion mechanisms of strain-induced martensite; (a) diffusion controlled and (b) shear type. Tomimura et al. [26, 27] reported the influence of the chemical composition i.e. Ni/Cr ratio and annealing temperature on the reversion mechanism. On the other hand, Takaki et al. [28] investigated the effect of the pre-cold working on the diffusion-controlled reversion of strain-induced martensite. These investigations also presented an insight into the microstructural modification induced by strain-induced martensite reversion to austenite. Takaki et al. looked into the type/morphology of strain-induced martensite that influenced the reverted austenite grain size. Johansen et al. [29] reported a detailed study on the influence of the aforesaid mechanisms on the microstructure of reversed austenite. The primary objective of this investigation was to explore or correlate the annealing temperature and the reversion mechanism to the formation of nano/submicron grain structure. A large annealing time (30 min) was used in these studies and the material studied was a commercial 301 type SS containing high carbon (0.09%). Therefore, many of the inferences were influenced by the two parameters mentioned above. The present study aims to address some of the issues, such as the role of martensite content and short annealing time on the microstructural modification of reverted austenite. Through short annealing time, an attempt has been made to capture the onset of microstructural changes just after the completion of martensite reversion. The material selected for the study was a commercial grade AISI 304L SS having carbon content much lower (0.023%) than AISI 301 SS. The annealing times were optimised to achieve just completion of phase reversion. An attempt has been made to capture the microstructure of the newly formed austenite before it goes through the subsequent recovery and recrystallisation process.

Experimental

Material and processing

Commercial AISI 304L SS plates of dimension 100 mm × 30 mm × 10 mm were solution treated at 1080 °C for 1 h and quenched in water to achieve chemical homogeneity. The chemical composition of the SS is presented in Table 1. A multi-pass unidirectional cold rolling with uniform thickness reduction per pass was performed in a two-high rolling mill with oil lubrication. The cold rolling was performed with an inter-pass cooling and without inter-pass cooling. The total reduction of thickness was of the order of 90% and the finished thickness of the plates was 1 mm. The cold-rolled samples were heat treated in the temperature range of 750–1000 °C, in a muffle furnace for durations of 90–600 s and were cooled in still air. The heat-treatment process will henceforth be referred to as annealing and is presented in Table 2. The starting annealing temperature of 750 °C was considered because it was found to be the recrystallisation temperature for 90% cold-rolled SS. The details of the effect of annealing temperature on recrystallisation were not included here.

Table 1 Chemical composition of the stainless steel

Element	C	Mn	Cr	Ni	Si	S	P	N
%wt	0.023	1.8	18.55	9.5	0.54	0.01	0.026	0.02

Structure and microstructure characterisation

The phase identification was performed by the X-ray diffraction (XRD) technique using Bruker AXS, D8, X-ray diffractometer. The quantitative estimation of the phases was performed using Rietveld analysis of the XRD data. In the Rietveld refinement, the observed-diffraction pattern was treated in its entirety and was compared to a theoretically calculated pattern. Several parameters were refined to fit the observed-diffraction pattern. The refined variables included microstructural parameters, peak shape parameters, instrumental broadening and sample absorption. The standard metallographic techniques were employed for the preparation of specimens for optical microscopy. To reveal the microstructure, specimens were etched with a solution of HCl (9 ml)–HNO_3 (3 ml)–CH_3OH (4 ml). For scanning electron microscope (SEM)-based electron backscattered diffraction (EBSD) study, the specimens were first prepared by standard metallographic techniques and were subsequently electro-polished in an electrolytic bath of 10 pct perchloric acid in acetic acid at 25 V and about 4 °C. Hitachi 3400 SEM attached with HKL EBSD system was used for the present investigation. The typical area analysed was 170 × 130 μm^2 and a minimum of four different areas were mapped. The pattern indexing quality was very high (90%). The transmission electron microscope (TEM) studies were performed on thin foils using Philips CM200 microscope at 200 kV operating voltage. These studies were mainly conducted on cold-rolled specimens to understand the type and morphology of strain-induced martensite in the two rolling processes. The initial thin foils parallel to the rolling surface were prepared by mechanical polishing. The final electrolytic thinning of the foils was done in acetic acid with 5% perchloric acid electrolytic bath. Vickers macro hardness measurement was carried out using Macro hardness tester, Reicherter Stiefelmayer UH-3, Germany, in as cold rolled and annealed specimens. A load of 30 Kg was used for all the measurements.

Table 2 Residual volume fraction of strain-induced martensite after annealing at various temperatures and time

Temperature, °C	Annealing time, s	Initial % strain-induced martensite		Residual % strain-induced martensite	
		Specimen I	Specimen II	Specimen I	Specimen II
750	600	43	89	10.2	9.5
800	600	43	89	9.5	8
850	300	43	89	8.5	8.5
900	120	43	89	9.5	8.5
950	120	43	89	8.5	7.5
1000	90	43	89	7.0	8.0

Results

Microstructural characterisation

The optical microstructure of the solution-annealed specimens and the cold-rolled specimens along the through thickness direction is presented in Fig. 1. The solution-annealed specimen exhibited typical polygonal grains microstructure of austenite with annealing twins, as shown in Fig. 1a. The cold rolling of the solution-annealed specimen up to about 90% thickness reduction resulted in the formation of a typical fibrous type structure. This type of structure is normally observed in heavily cold-worked materials. Figure 2 shows a representative TEM micrograph of 90% cold-rolled inter-pass cooling specimen. The microstructure broadly consists of two very distinct regions: (i) regions of blocky dislocated tangles and (ii) regions of banded structure, as shown by the arrows in Fig. 2. Most of these regions were identified as strain-induced martensite by the selected area diffraction pattern analysis. In general, the morphology of strain-induced martensite for the two rolling processes appeared to be similar.

Structural characterisation by XRD

Figure 3 shows the X-ray diffraction pattern of the cold-rolled and annealed samples at various temperatures. The

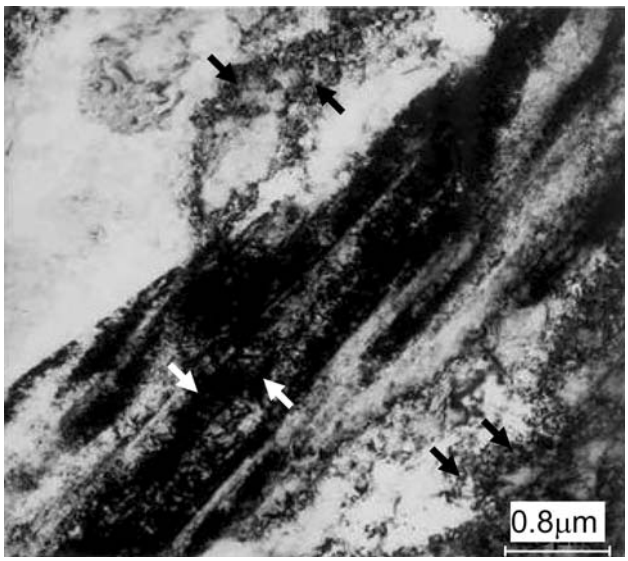

Fig. 2 TEM of cold-rolled SS showing banded structure as shown by *white arrows* and blocky dislocated structure as shown by *black arrows* of strain-induced martensite

cold-rolled specimens exhibited both martensite and austenite phases. The cold rolling by without inter-pass cooling route resulted in 43% of the volume fraction of strain-induced martensite whereas the inter-pass cooling route produced 89% volume fraction of strain-induced martensite because of the strain-induced phase transformation. The difference in strain-induced martensite volume

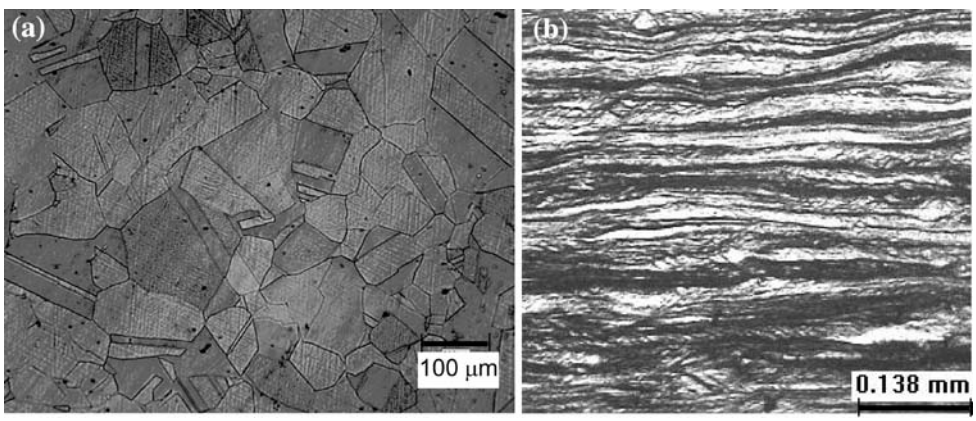

Fig. 1 Optical microstructure showing **a** polygonal grains of austenite along with annealing twins after solution annealing and **b** fibrous structure in cold-rolled specimen 0.8 μm

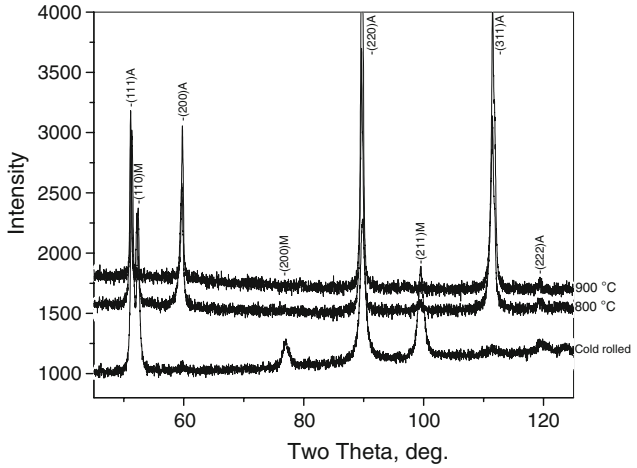

Fig. 3 X-ray diffractogram depicting formation of strain-induced martensite by multi-pass cold rolling without inter-pass cooling and its reversion after annealing. *A* Austenite, *M* Martensite

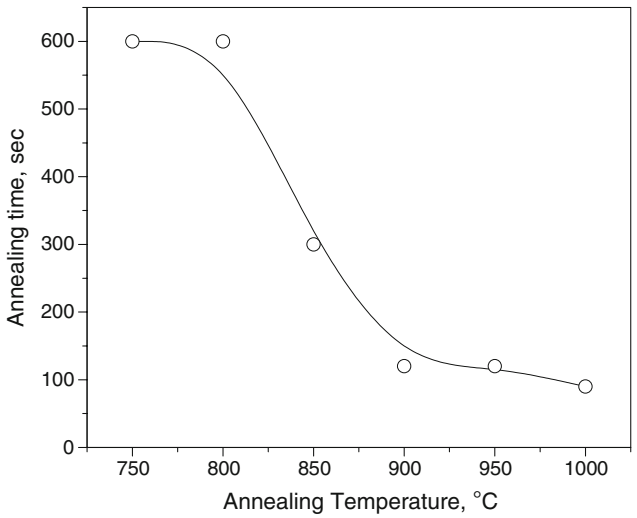

Fig. 4 Effect of annealing time and temperature on the reversion behaviour of SIM

fraction was due to the adiabatic heating of the sample during rolling. The highest temperature (M_d), at which martensite forms due to deformation, was calculated from the empirical equation proposed by Angle [38]. For this type of SS, it was around 28 °C. Therefore, the adiabatic heating of rolling resulted in a lower volume fraction of strain-induced martensite in without inter-pass cooling. The annealing at various temperatures resulted in the reversion of strain-induced martensite. The effect of annealing time and temperature on phase reversion is shown in Fig. 4 and is also presented in Table 2. The reversion time to obtain a near full austenitic microstructure was found to obey a sigmoidal type relation with temperature. The plot was deduced from several annealing temperatures at various time intervals till the volume fraction of the austenite phase was more than 90%.

SEM-EBSD analysis

The cold-rolled specimens could not be subjected to EBSD analysis due to their highly strained conditions. Therefore, the EBSD analysis was used to study the specimens after the annealing treatment. A representative orientation map (OM) of the specimens annealed at 800 and 950 °C is depicted in Figs. 5 and 6, respectively. The yellow lines in the OM represent low angle boundaries (LAB) with grain boundary misorientation below 15°. As expected, the microstructure showed the formation of fine grains at low temperatures and relatively larger grains at high temperatures of annealing in inter-pass cooling route. On the contrary, without inter-pass cooling route resulted in the formation of fine grains at high temperatures and larger grains at low temperatures of annealing. This was quite contrary to the conventional recrystallisation and the grain growth concept, which predicts that higher the temperature larger the grain size. From OM, the grain size distribution was determined by selecting the misorientation criteria above 15° for a grain boundary. This is illustrated as a

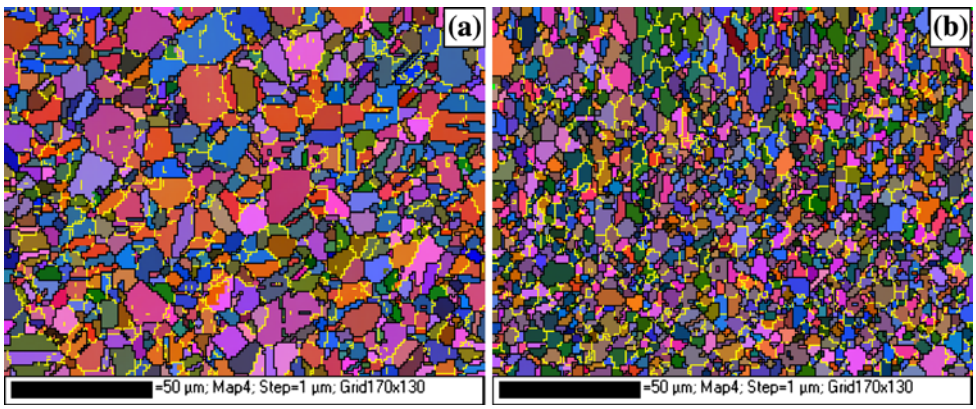

Fig. 5 Orientation maps of without inter-pass cooling specimen annealed at **a** 800 °C for 5 min and **b** 950 °C for 2 min. The *yellow lines* represent low angle grain boundaries with misorientation below 15°

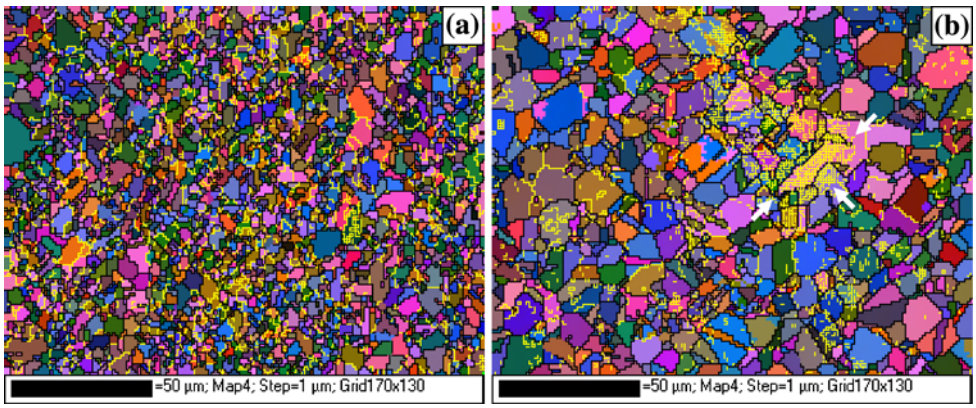

Fig. 6 Orientation map of inter-pass cooling specimens annealed at **a** 800 °C for 5 min and **b** 950 °C for 2 min. Large block of reverted austenite inundated with LABs, as shown in *yellow colour*, is highlighted by *arrows*

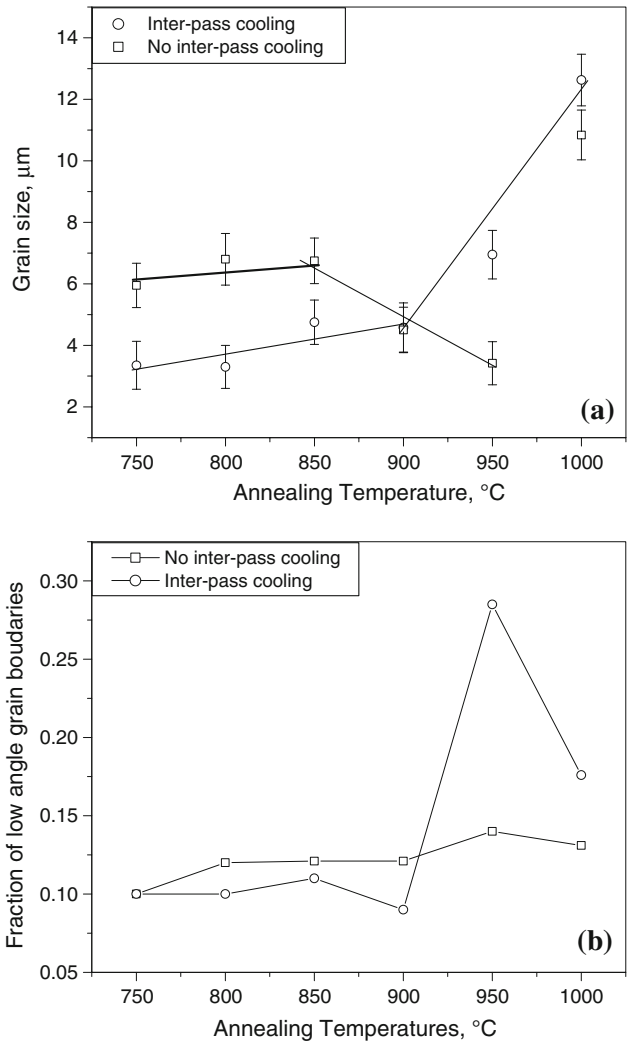

Fig. 7 Variation in **a** average grain size distribution and **b** low angle boundaries below 15° after annealing of the 90% cold-rolled stainless steel

function of temperature in Fig. 7. The grain size distribution did not show an increasing trend with increasing annealing temperatures. The plot showed two very distinct straight lines of slopes of varying magnitude. At low temperatures, both the process routes showed a small grain size variation of ~3–5 µm for inter-pass cooling and ~6–7 µm for without inter-pass cooling. It was observed that the grain size of the microstructure formed by without inter-pass cooling route was nearly double than that of the microstructure formed by inter-pass cooling route. At temperatures above 900 °C, there was a sharp increase in the grain size (~5–12 µm) indicating a grain growth for inter-pass cooling process. Contrary to this, without inter-pass cooling specimen behaved in an abnormal manner, showing a negative slope between 850 and 950 °C. The grain size decreased from ~6 to 3 µm and then increased. Further, a fraction of LAB's i.e. those below 15°, present in the austenite phase is shown in Fig. 7b. The LAB's were found to increase slightly with the annealing temperatures for without inter-pass cooling. The inter-pass cooling route on the other hand, produced a sharp increase in the LABs above 900 °C.

Hardness

The Vicker hardness measurements on cold-rolled and annealed specimen showed softening with increasing annealing temperatures as depicted in Fig. 8. However, the decrease in the hardness did not follow a straight line path. Inter-pass cooling route showed first the initial sharp softening trends (~215–180 Hv) between 750 and 850 °C during annealing and then retarded decrease in hardness (~180–160 Hv) up to 950 °C. The annealing at 1000 °C resulted in a sudden decrease of hardness to a value of 134 Hv. On the other hand, without inter-pass cooling showed an initial rapid decrease in the hardness from ~200–150 Hv. Here again there was a change in the hardness trend as shown in the Fig. 8. Similar to the changes observed in the grain size with annealing temperature, the hardness also showed higher values at 950 °C and then lower values. The hardness vs. temperature plot very distinctly depicted different trends in various annealing temperature regimes. The changes in the hardness were found to match well with the changes in the microstructure.

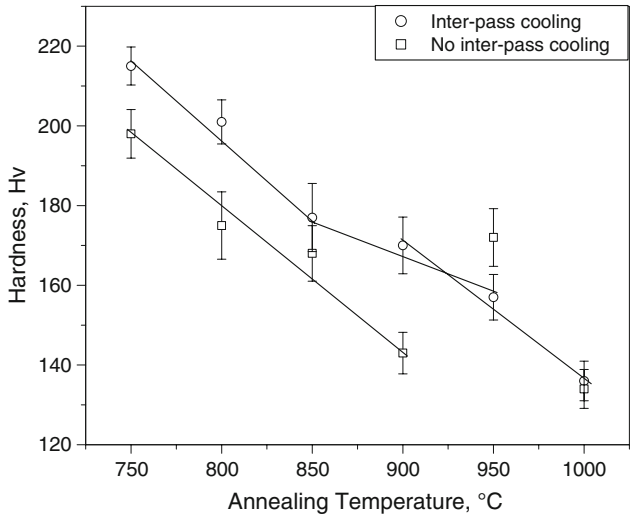

Fig. 8 Variation in macro hardness after annealing of the 90% cold-rolled stainless steel

Discussion

The volume fraction of strain-induced martensite dropped steeply with increasing annealing temperatures and then stabilized, as shown in Fig. 4. At lower temperatures, longer annealing time was taken for the complete reversion of strain-induced martensite as compared to the higher temperatures. This, initially, appears as typical diffusion-controlled phenomena. At very low temperatures, the reaction rate, whether it is nucleation or growth, becomes small because the diffusion rate always decreases rapidly with decreasing temperatures and accelerates as the temperature is raised above the transformation temperature. The effect of the two processing routes (without inter-pass cooling and inter-pass cooling) of stainless steel on the evolution of the final austenite microstructure was observed to be different. The inter-pass cooling produced fine grains compared to without inter-pass cooling at lower temperatures of annealing for the same annealing time, as depicted in Figs. 5 and 6. However, both the process routes showed a very small grain growth with increasing temperature in the range of 750–850 °C. This was mainly because austenitic stainless steels do not exhibit high grain-growth rate at these temperatures [30]. Of the two processing routes, inter-pass cooling exhibited a finer grain size. It may possibly be attributed to the larger volume fraction of strain-induced martensite (89%), which promotes a higher nucleation rate [26, 28, 29]. Hence, one may conclude that at lower annealing temperatures the increasing volume fraction of strain-induced martensite was more efficient for the formation of fine-grained austenitic microstructure. It was observed that above 900 °C, there was a rapid rise in the grain size, through the inter-pass cooling route, while without inter-pass cooling exhibited a sharp decrease in the grain size and then a rise. The increase in the final grain size at temperatures above 850 °C was previously reported as a result of change in the phase reversion mechanism [26–29]. The explanation put forth for this was the initiation of the shear-type reversion mechanism or shifts from one mechanism to another at higher temperatures [26–37]. Thermodynamically for the shear mechanism to be operative a minimum energy is required and Tomimura et al. reported the lowest possible temperature as 750 °C [27]. In case of shear mechanism, strain-induced martensite would first revert to the dislocated austenite laths having large fractions of LABs within it. Then the newly reverted lath austenite would subsequently undergo recovery and recrystallisation. This would lead to a strain-free equiaxed austenite grain formation. The stress generated by the austenite to strain-induced martensite transformation favours the reverse shape change during strain-induced martensite to reversed austenite and reversion leading to a large single crystal of austenite [38]. The new reversed austenite crystal is made up of subcrystals with slightly different misorientation. Such a reversed austenite block inherits a high defect density of strain-induced martensite and manifests in the form of an increase in the low angle boundary. The subsequent annealing process occurs through the recovery and recrystallisation of these large lath austenite blocks and may result into relatively coarser austenite grains. An increase in the LABs as shown in the Fig. 7b supported this hypothesis. A large austenite block inundated with LAB, shown by arrows in Fig. 6b, may be the result of the dislocation substructure inherited from strain-induced martensite during the reversion by shear. The evolution of the microstructure in the specimen consisting of 89% of the volume fraction as strain-induced martensite was observed to behave as reported in the previous investigations [26–29]. On the other hand, the specimen with 43% of the volume fraction of strain-induced martensite was found to behave somewhat differently.

The specimens with 43% of strain-induced martensite showed an initial increase in the grain size up to 900 °C and then a decrease in the size at 950 °C. The smaller grain size obtained at an annealing temperature of 950 °C was contrary to the expectation. This was because of the dependence of the average grain-growth rate on the annealing temperature and time as represented in the following equation [39]

$$G^{\mathrm{G}}(t) = C_{\mathrm{G}}\, t^{-n} \exp\left(-\frac{Q_{\mathrm{G}}}{RT}\right) \tag{1}$$

where C_{G} is a constant, Q_{G} is the activation energy of interface migration and n is an exponent associated with

decrease of driving force with annealing time, t, i.e. the stored energy, R is a gas constant and T is temperature. The possible argument for this could be the heterogeneity in nucleation and growth behaviour due to the spatial stored energy variation, which is a function of cold deformation and also of matrix phase. The microstructure here consists of a highly deformed austenite and a near equal volume fraction of strain-induced martensite. Thus, a non-homogenous distribution of stored energy results in varying recrystallisation kinetics spatially. During the annealing cycle the nuclei per unit area would be governed by the prior deformed regions and the interface boundary area between the austenite and strain-induced martensite. On the other hand, once the nucleation of the austenite grain takes place, its growth rate determines the final grain size distribution. The equations above show the temperature and time dependency. Therefore, to attain a small average grain size and its distribution, it is necessary to accelerate the nucleation rate and retard the grain growth. The conditions prevailing at 950 °C appear to be more favourable for the fine grain formation.

During annealing, the residual heavily deformed austenite was subjected to recovery and recrystallisation, whereas strain-induced martensite went through a phase transformation, through diffusion or shear mechanism, to reverted austenite. Further, the changes in the reverted austenite were governed by the recovery and recrystallisation process. At low temperatures the microstructural changes in both the phases were governed by the diffusion process. Therefore, the larger grain size, presumably at lower annealing temperatures, was due to the longer annealing durations. Hence, the time to complete the phase reversion at these temperatures was longer than desired. On the contrary, the presence of strain-induced martensite was expected to support the fine grain formation. This may have been possible because of the distribution of strain-induced martensite in the microstructure. The wide spread distribution of strain-induced martensite due to the smaller fraction may not be effective for grain refinement. At 950 °C, the fine grains may have formed as a result of the high rate of recrystallisation of the highly deformed austenite and the newly reverted austenite with a high defect density. The shear reversion mechanism operating at this temperature must be inducing a high defect density in reverted austenite. Another influencing factor may be the interface boundary area between the austenite and strain-induced martensite. The presence of these boundaries may accelerate the nucleation rate at a critical annealing temperature. These boundaries were, however, expected to be consumed very quickly due to the phase transformation of strain-induced martensite. These conclusions were speculative in the absence of the in situ observations and were based on the fundamental understanding of the recrystallisation and growth mechanism.

The microstructure changes were mostly reflected on the hardness values. The continuous softening up to 900 °C was mainly due to the recovery and recrystallisation phenomenon. The retarded rate of decrease in the hardness could be attributed to the increase in the LABs originating from the shear-type reversion mechanism.

Conclusions

The cold-rolled 304L stainless steel specimens processed by two different rolling conditions resulted in the formation of fine grain-sized microstructure depending on the annealing temperature. A high volume fraction of martensite in the austenite matrix was observed to promote the formation of fine grained microstructure at low annealing temperatures, below 900 °C. On the other hand, a critical annealing temperature and time were necessary for the formation of fine grained microstructure in specimens having smaller fractions of strain-induced martensite. Further, the observed annealing temperature was above 900 °C in specimens with low volume fraction of strain-induced martensite. The difference in annealing temperature for the evolution of fine grained microstructure in the two specimens was attributed to the phase reversion mechanism of strain-induced martensite. The formation of fine grained microstructure in the specimen with large volume fraction of strain-induced martensite was correlated to the diffusion controlled reversion mechanism. On the other hand, it was mainly the heterogeneity in nucleation and growth behaviour due to spatial stored energy variation in the specimens with smaller fraction of strain-induced martensite. The fine austenite grains formed at lower temperatures and high temperatures may have possible implications on the properties. However, this could not be clearly brought out by the hardness measurements.

Acknowledgements The authors are grateful to Director, National Metallurgical Laboratory, for supporting this work. The authors also wish to record their gratitude to Sri P.K De for his support in conducting the experiments.

References

1. Valiev RZ, Sergueeva AV, Mukherjee AK (2003) Scr Mater 49:669
2. Alexandrov IV, Valiev RZ (2001) Scr Mater 44:1605
3. Stolyarov VV, Zhu YT, Lowe TC, Islamgaliev RK, Valiev RZ (1999) Nanostruct Mater 11:947
4. Valiev RZ (1997) Mater Sci Eng A 234:59
5. Segal VM (1999) Mater Sci Eng A 271:322
6. Fukuda Y, Oh-ishi K, Horita Z, Langdon TG (2002) Acta Mater 50:1359
7. Kim J, Kim I, Shin DH (2001) Scr Mater 45:421
8. Shin DH, Kim I, Kim J, Park KT (2001) Acta Mater 49:1285

9. Horita Z, Furukawa M, Nemoto M, Langdon TG (2000) Mater Sci Technol 16:1239
10. Zhu YT, Lowe TC (2000) Mater Sci Eng A 291:46
11. Saito Y, Utsunomiya H, Tsuji N, Sakai T (1999) Acta Mater 47:579
12. Tsuji N, Ueji R, Minamino Y (2002) Scr Mater 47:69
13. Tsuji N, Saito Y, Utsunomiya H, Tanigawa S (1999) Scr Mater 40:795
14. Inoue T, Torizuka S, Nagai K (2001) International Symposium on Ultrafine grained Steels (ISUGS 2001). The Iron and Steel Institute of Japan, Fukuoka, Japan, p 88
15. Kaspar R, Distl JS, Pawelski O (1988) Steel Res 59:421
16. Hodgson PD, Hickson MR, Gibbs RK (1999) Scr Mater 40:1179
17. Mabuchi H, Hasegawa T, Ishikawa T (1999) ISIJ Int 39:477
18. Yang ZM, Wang RZ (2003) ISIJ Int 43:761
19. Choi JK, Seo DH, Lee JS, Um KK, Choo WY (2003) ISIJ Int 43:746
20. Matsumura Y, Yada H (1987) ISIJ Int 27:492
21. Son YI, Lee YK, Park K-T, Lee CS, Shin DH (2005) Acta Mater 53:3125
22. Park K-T, Han SY, Ahn BD, Shin DH, Lee YK, Um KK (2004) Scr Mater 51:909
23. Ueji R, Tsuji N, Minamino Y, Koizumi Y (2002) Acta Mater 50:4177
24. Tsuji N, Ueji R, Minamino Y, Saito Y (2002) Scr Mater 46:305
25. Tomimira K, Takaki S, Tanimoto S, Tokunaga Y (1991) ISIJ Int 31:721
26. Tomimura K, Takaki S, Tokunaga Y (1991) ISIJ Int 31:1431
27. Takaki S, Tomimura K, Ueda S (1994) ISIJ Int 34:522
28. Johannsen DL, Kyrolainen A, Ferreira PJ (2006) Metall Trans A 37:2325
29. Di Schino A, Barteri M, Kenny JM (2002) J Mater Sci Lett 21:751
30. Ma Y, Jae-Eun J, Young-Kook L (2005) Scr Mater 52:1311
31. Smith H, West DRF (1973) J Mater Sci 8:1413. doi: 10.1007/BF00551664
32. Guy KB, Butler EP, West DRF (1983) Met Sci 17:167
33. Haebner F, Plaut RL, Padilha AF (2003) ISIJ Int 43:1472
34. Montanari R (1990) Z Metallkd 81:114
35. Breedis JF (1966) Trans Metal Soc AIME 236:218
36. Mirzadeh H, Najafizadeh A (2009) Mater Des 30:570
37. Angel T (1954) J Iron Steel Inst 177:165
38. Nishiama Z (1978) Martensitic transformation. Academic Press, New York
39. Kozeschnik E, Pletenev V, Zolotorevsky N, Buchmayr B (1999) Metall Trans A 30:1663